IOP Publishing and International Atomic Energy Agency Nuclear Fusion
Nucl. Fusion **51** (2011) 113019 (10pp) doi:10.1088/0029-5515/51/11/113019

L–H threshold studies in NSTX

S.M. Kaye[1], R. Maingi[2], D. Battaglia[2], R.E. Bell[1], C.S. Chang[1,3], J. Hosea[2], H. Kugel[2], B.P. LeBlanc[2], H. Meyer[4], G.Y. Park[3,5] and J.R. Wilson[1]

[1] Princeton Plasma Physics Laboratory, Princeton University, Princeton, NJ 08543, USA
[2] Oak Ridge National Laboratory, Oak Ridge, TN 37831, USA
[3] Courant Institute of Mathematical Sciences, New York University, New York, NY, USA
[4] CCFE, Culham Laboratory, Abingdon, UK
[5] Korea Superconducting Tokamak Advanced Research (KSTAR), National Fusion Research Institute, Daejeon, Korea

E-mail: skaye@pppl.gov

Received 27 December 2010, accepted for publication 9 June 2011
Published 28 October 2011
Online at stacks.iop.org/NF/51/113019

Abstract
Recent experiments in the low aspect ratio National Spherical Torus Experiment (NSTX) have been run in support of the high priority ITER and ITPA issue of access to the H-mode. Specifically, a series of experiments showed reduced power threshold values for deuterium versus helium plasmas, and for plasmas with lower current, lower triangularity and with lithium conditioning. Application of $n = 3$ fields at the plasma edge resulted in higher power thresholds. To within the constraints of temporal and spatial resolutions, no systematic difference in T_e, n_e, p_e, T_i, v or their derivatives was found in discharges that transitioned into the H-mode versus those at slightly lower power that did not. Finally, $H_{98y,2} \sim 1$ confinement quality could be achieved for powers just above the threshold power in ELM-free conditions.

1. Introduction

Attempts to characterize and understand the physics of the L-mode to H-mode transition have been at the forefront of tokamak physics studies since the H-mode was discovered in 1982 [1, 2]. Initial experimental studies focused on global parametric dependences for the heating power required for transition into the H-mode, such as those on density, plasma current, toroidal field and plasma size in conventional aspect ratio tokamaks. These studies led to the development of parametric scalings in support of the development of the ITER physics basis [3, 4]. Later, additional experimental studies focused on the effect of the magnetic configuration and the ion ∇B-drift direction on the L–H power threshold, P_{LH} [5]. These experimental studies indicated a large range of heating power even for similar global discharge parameters, thus indicating the importance of other, as yet unquantified parameters. Experimental studies extended into low aspect ratio [6] and examined the role of edge parameters and their gradients. In this latter area, several experiments (C-Mod, ASDEX-U and JET) identified the edge electron temperature as having a critical threshold for an L–H transition [7–10]. Studies on DIII-D showed that ∇T_e and ∇T_i (and thus ∇p_e and ∇p_i) increased during the L-phase for discharges that ultimately transitioned into the H-mode [11]. Further, studies of scrape-off layer flows in C-Mod showed that with unfavourable ∇B-drift, there was counter-current rotation in the plasma core, and this led to higher threshold powers [8]. Despite these results, the observations of threshold edge parameters or their gradients have not been universal. There are other effects, such as plasma shape and wall conditioning that can also affect the power required for an L–H transition.

Theory also attempted to explain the L–H transition [12, and references therein], but no single theory emerged. It is generally believed that edge $E \times B$ shear, through mean or zonal flows, is important in turbulence suppression that can lead to the L–H transition [13, 12, and references therein]. There has also recently been some more evidence of the importance of zonal flows in the L–H transition [14–17], but this is still an area of active experimental research and validation of theory.

Knowing the characteristics, and more importantly the underlying physics, of the L–H transition has been identified by the ITER Physics group as a high priority issue. Operation in the H-mode is critical to the success of ITER, and knowledge of the transition characteristics beyond what is already known was requested in order to be able to refine the expectations for ITER with more precision. In this work, we report results of dedicated experiments carried out in the National Spherical Torus Experiment (NSTX) in support of the high priority ITER and ITPA needs, addressing such issues as effect of plasma ion species, applied 3D fields, wall conditioning, plasma current and plasma shape/X-point position on the L–H power threshold (P_{LH}) and local parameters leading up to the transition. NSTX

is a low aspect ratio tokamak with $R/a = 0.85/0.65\,\mathrm{m} \sim 1.3$, which operates with neutral beam and high harmonic fast wave (HHFW) heating powers up to 7 MW and 4 MW, respectively. NSTX typically operates at toroidal fields of B_T up to 0.55 T, plasma currents I_p of up to 1.4 MA, with elongations κ up to 3 and triangularity δ up to 0.8. NSTX has implemented an external coil set capable of applying $n = 1$ to 3 fields at the plasma edge [18], and it also has conditioned the plasma-facing graphite tiles with evaporated lithium [19].

Experiments on the species effect revealed that the L–H threshold power for helium is approximately a factor of 1.25 to 1.6 greater than that for deuterium, and there is no evidence of hysteresis for L–H versus H–L transitions. There was a 35% reduction in the threshold power normalized by line-averaged density for discharges using lithium evaporation to coat the plasma-facing components than for those that did not. Application of largely non-resonant $n = 3$ fields at the plasma edge resulted in about a 65% increase in density-normalized threshold power with little difference in plasma rotation at the outermost measurement location. Normalized threshold powers are almost a factor of two greater at 1 MA than at 0.7 MA, consistent with XGC0 [20] neoclassical calculations showing a deeper E_r well and stronger E_r shear near the edge for lower current. Also consistent with XGC0 predictions of the effect of x-point radius, experiments indicated that low triangularity discharges required the lowest P_LH to transition into the H-mode. To within the constraints of temporal and spatial resolutions, no systematic difference in T_e, n_e, p_e, T_i or their derivatives was found in discharges that transitioned into the H-mode versus those at slightly lower power that did not. Finally, it was found that both RF and NBI-heated discharges could attain values of $H_{98y,2} \sim 1$ under ELM-free conditions for powers just above the power threshold.

The outline of the paper is as follows. The experimental results of power threshold parametric dependences, along with neoclassical calculation results where possible, will be presented in section 2. The evolution of local parameters and their gradients leading up to the L–H transition is presented in section 3, and the confinement quality of the H-phase discharges with powers near the threshold power is examined in section 4. The summary is given in section 5.

2. L–H threshold power dependences

2.1. Effect of plasma species

Since initial ITER operations will probably be with either hydrogen or helium plasmas, it is important to understand how the L–H power threshold scales with working gas species. Dedicated studies of this dependence were performed in ASDEX-Upgrade, using both electron cyclotron (EC) and neutral beam injection (NBI) heating in deuterium and helium plasmas [21]. A direct comparison between pure deuterium and helium plasmas was made for the EC heating cases. The experiments showed no difference in power threshold for the two species. Furthermore, the density for which the power threshold is a minimum was also found to be similar for the two species. Dedicated experiments were performed in NSTX to follow up on this initial work. The NSTX experiments utilized HHFW, which allowed the studies to be performed

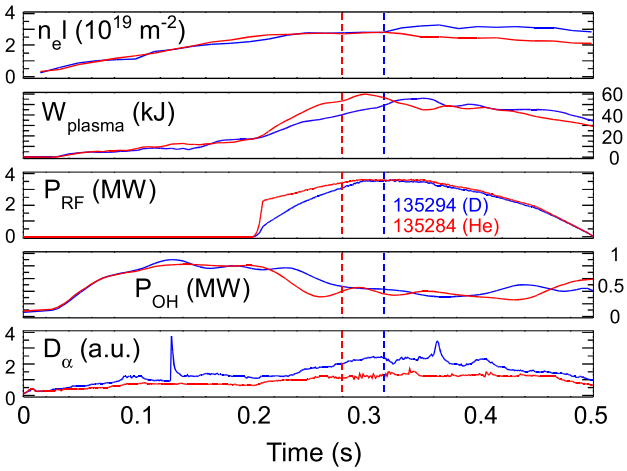

Figure 1. Line integral density, plasma stored energy, HHFW heating power at the antenna, ohmic heating power and D_α emissivity for 0.65 MA, 0.54 T deuterium (blue) and helium (red) plasmas. The colour-coded vertical lines indicate the time of the L–H transition for each species.

also in relatively pure deuterium and helium plasmas. The HHFW, with a wavenumber of $k_\phi = -8\,\mathrm{m}^{-1}$, was injected with a power waveform that increased up to 3.5 MW power at the antenna, flattoped at that value for approximately 60 ms, then decreased. This power waveform allowed a precise determination of both the L–H and H–L transitions.

The time evolution of a helium (He) and a deuterium (D) discharge in this study is shown in figure 1. In the figure, the time rate of change of the density in the deuterium discharge (blue) was seen to increase at 0.1 s. This is due to additional gas fuelling starting at that time. The D_α spike in the D discharge at 0.13 s was due to a transient configuration change, and it indicated increased plasma–wall interactions. The L–H transition in the D discharge occurred at 0.31 s, as indicated by the drop in the D_α emission for this discharge. The L–H transition occurred at 0.29 s in the He discharge; this time was determined as described below. In both cases, the transition occurred at or near peak HHFW power. While the density increased after the L–H transition in the D discharge, no increase was seen in the He discharge. The ohmic power was comparable for the two cases at the respective times of transition, and the stored energy started to decrease as the heating power was reduced shortly after (30 to 50 ms) the transition. No H–L back transition was evident in the D discharge.

In helium discharges, the L–H transition could not be determined by the D_α drop; instead, careful analysis of the change in edge density profile was used to determine both the forward and backward transitions. An example of this is shown for a helium plasma in figure 2. It is clear in this figure that the evolution of the T_e and n_e profiles are good indicators of the L–H or H–L transitions. The L–H transition is reflected by the increase in gradients (top panels), while the H–L transition is reflected by the decrease in gradients (bottom panels). Since the time resolution of these measurements is 16 ms, the time of the transition is known only to this accuracy.

To determine L–H and H–L transition powers, the actual HHFW power that heated the plasma had to be determined. To

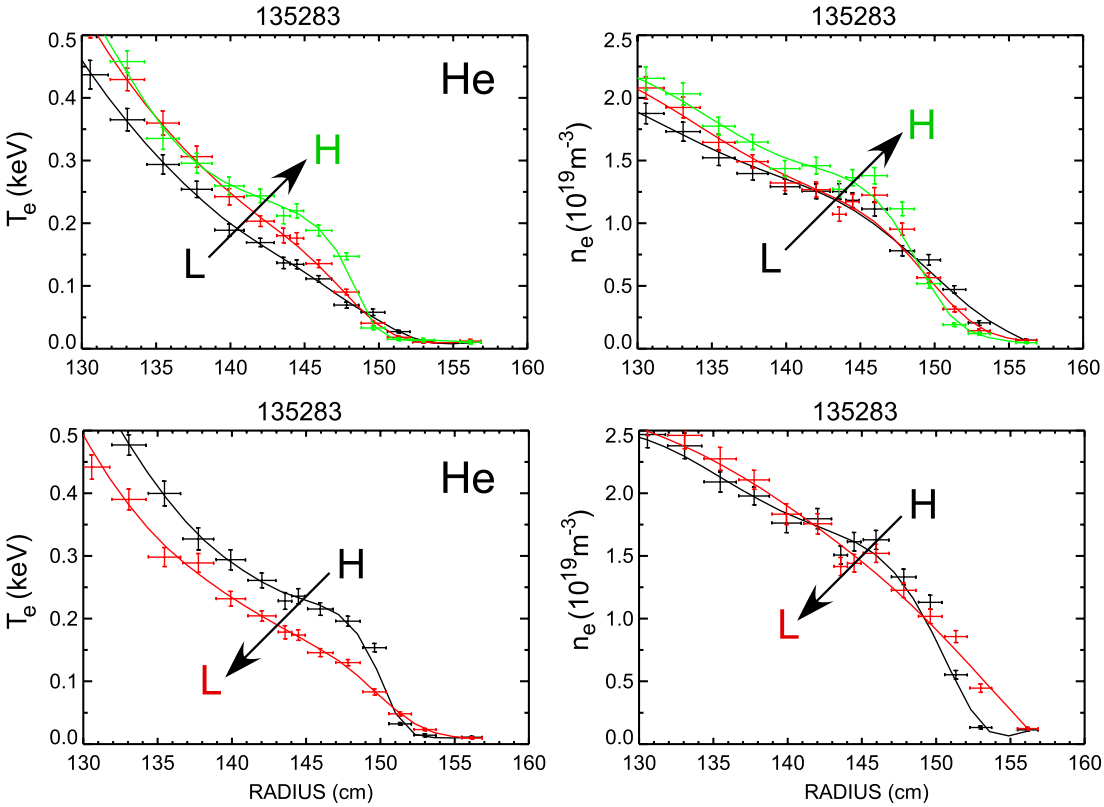

Figure 2. Evolution of the T_e and n_e profiles through the L–H transition (top panels), and similarly for the H–L back transition (bottom panel). These changes were used to determine the transition times in helium plasmas. The solid curves are spline fits to the data. The times at which the profiles were measured were 0.248 s (black), 0.265 s (red) and 0.29 s (green) in the upper panels and 0.398 s (black) and 0.43 s (red) in the lower panels.

do this, a perturbation method was used which took advantage of occasional dropouts of the HHFW power. From the time rate of change of plasma stored energy and the ultimate level of energy to which the plasma relaxed after the power dropout, this net heating power could be estimated. For the range of discharges studied, the average efficiency, defined as the ratio of the calculated (i.e. net) heating power to the power at the antenna, was approximately 0.30 ± 0.11, with slightly higher efficiencies for helium (0.33) than for deuterium (0.28). The loss power, or power through the separatrix, was defined as this heating power plus the ohmic power less the time rate of change of stored energy at the time of the transition, $P_{\rm loss} = P_{\rm net,RF} + P_{\rm OH} - {\rm d}W/{\rm d}t$. The loss power at which the discharge transitioned into the H-mode is designated as $P_{\rm LH}$.

The set of discharges used to study the threshold powers exhibited a small range of densities, with the line-averaged density varying from 1.8×10^{19} to 2.2×10^{19} m^{-3} at the time of the L–H transition (most of the discharges were within a 15% range). Figure 3 shows the density dependence of the total net heating power, $P_{\rm net} = P_{\rm RF,net} + P_{\rm OH}$ (left panel) and the loss power (right panel). The heating powers as functions of density at the L–H transition are shown by solid symbols (helium in red, deuterium in blue), while that for the H–L transition is shown by the open symbols. An increase in power at the L–H transition with density is seen for both power definitions, and within the small range of density, the scaling of the powers is not inconsistent with either a linear dependence or the $n_e^{0.75}$ dependence seen in L–H power threshold scalings [4]. It is also seen that while $P_{\rm net}$ is comparable for D and He (left panel), $P_{\rm loss}$ is higher for He than for D at similar densities (right panel). This will be discussed more below. For each species, $P_{\rm loss}$ increases with increasing density. The H–L transitions do not exhibit as clear a density dependence, especially for $P_{\rm net}$, as the L–H transitions. It should further be noted that experiments have not yet been run to identify the critical density for the minimum $P_{\rm LH}$ for either species. Proximity to this critical density could affect the relation between the $P_{\rm LH}$ values for D and He [22, 23].

Knowing the dependence of $P_{\rm LH}$ on density is important when comparing threshold powers at different densities, which is the case in some of the comparisons shown in this work. Therefore, the L–H threshold power will be normalized by n_e, assuming a linear dependence for simplicity, and this normalized power will be discussed in addition to the absolute power. Normalizing by $n_e^{0.75}$ instead of n_e would make little difference to the results since the range of densities is small.

The results of this isotope scan are shown in figure 4, where the power threshold normalized by the line-averaged density is plotted versus discharge number from a sequence of discharges. The results indicate that the L–H power threshold is approximately 20–40% greater in helium than in deuterium. The error bars reflect the uncertainty primarily in the determination of the heating efficiency overall, as well as for the differences in efficiency between deuterium and helium (indicated by the two symbols for each discharge, one representing the average efficiency and the other representing

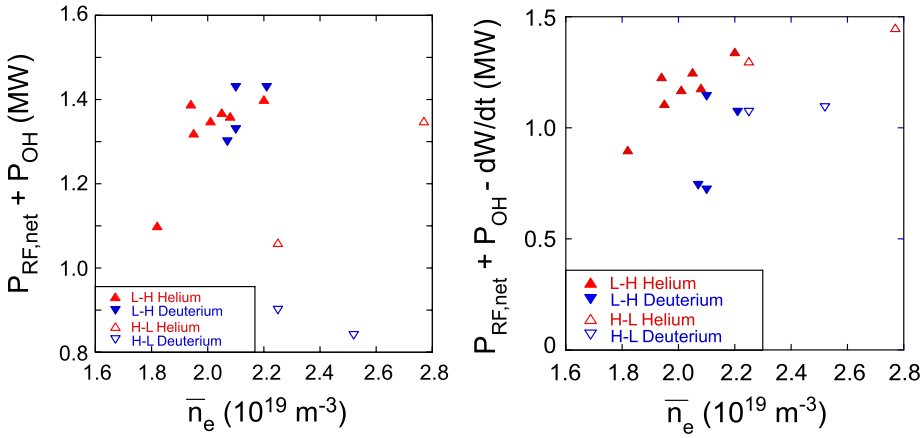

Figure 3. Net heating power, $P_{\mathrm{RF,net}} + P_{\mathrm{OH}}$ (left panel) and P_{loss} (right panel) as functions of line-averaged density for L–H transitions (solid symbols) and H–L transitions (open symbols) for helium (red) and deuterium (blue) discharges.

the efficiency for that particular species). As can also be seen by the open symbols, the H–L transitions occurred essentially at the same power level as the L–H transitions, indicating no hysteresis within this parameter range. It is interesting to note that in NSTX the difference in the threshold powers for helium and deuterium is near zero if the $\mathrm{d}W/\mathrm{d}t$ term is omitted from the definition of P_{LH}, with the threshold power being merely the sum of the HHFW heating and ohmic powers ($P_{\mathrm{RF,net}} + P_{\mathrm{OH}}$). Using this definition, there would also be a clear indication of hysteresis, with the H–L transition occurring at significantly lower normalized power than the L–H transition. This means that once in the H-mode, the discharge is able to remain there even with heating powers, defined in this fashion, lower than that required for entry. The difference between the results for the two definitions of power at the transition indicates the effect of the range of $\mathrm{d}W/\mathrm{d}t$ in these discharges. The $\mathrm{d}W/\mathrm{d}t$ was approximately a factor of two greater for deuterium than for helium, and for deuterium it could be up to a 30% to 40% effect on P_{LH}. It will be important in the future to perform these experiments holding the $\mathrm{d}W/\mathrm{d}t$ term as fixed as possible, and similar, for both deuterium and helium.

2.2. *Effect of applied magnetic perturbations*

Another key dependence studied in NSTX was that on applied edge magnetic perturbations. NSTX is equipped with a set of external coils able to generate magnetic perturbations with toroidal mode numbers from 1 to 3, with field amplitudes of several Gauss at the plasma edge [18]. These coils have been used for error field correction, low-n edge mode control and controlled generation of ELMs (they were not effective in suppressing ELMs). The importance of this study is related to the possible need for ELM control coils in ITER. The question to answer is whether the magnetic perturbations can be applied prior to the L–H transition in order to suppress even the first ELM that might be driven unstable once the ITER plasma is in the H-mode, without affecting P_{LH}. Dedicated experiments using $n = 3$ applied fields were performed in NSTX, and the results are shown in figure 5. Neutral beams were used to heat the plasma in these discharges. In the neutral beam heated plasmas, the loss power is defined to be $P_{\mathrm{loss}} = P_{\mathrm{b,i}} + P_{\mathrm{b,e}} + P_{\mathrm{OH}} - \mathrm{d}W_{\mathrm{e+i}}/\mathrm{d}t$. Here, $P_{\mathrm{b,i}}$ and $P_{\mathrm{b,e}}$ are the

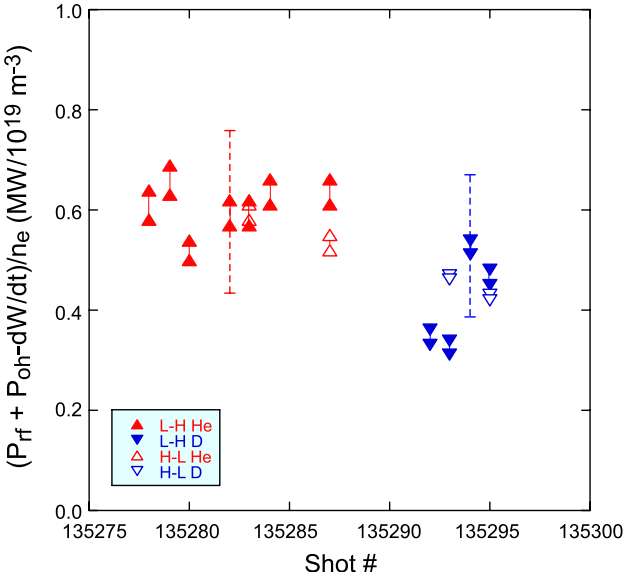

Figure 4. Threshold powers normalized by line-averaged density for a sequence of discharges. Error bars indicate the overall uncertainty in the heating efficiency. There are two symbols for each discharge, indicating the value using the average overall heating efficiency and the heating efficiency for that particular species.

beam collisional heating to the ions and electrons respectively. The figure compares two discharges, in blue and red, for which $n = 3$ fields were applied, with a baseline discharge in black in which no additional $n = 3$ field was applied (see $n = 3$ coil current in bottom panel). Some finite $n = 3$ current was needed for dynamic error field correction in all discharges. The baseline discharge, without additional applied $n = 3$ fields, showed a power threshold of approximately 1.4 MW (and power threshold normalized to plasma density of $0.55\,\mathrm{MW}/10^{19}\,\mathrm{m}^{-3}$), as compared with the power threshold of 2.6 MW and normalized threshold of $1.0\,\mathrm{MW}/10^{19}\,\mathrm{m}^{-3}$. Note that the power threshold is determined using the fact that the discharge in red remained in L-mode, while the one in blue, at slightly higher power, transitioned into the H-mode.

A comparison of the toroidal velocities as measured by C VI emission for the two discharges with $n = 3$ fields applied is shown in (figure 6). The plot shows both the measured data

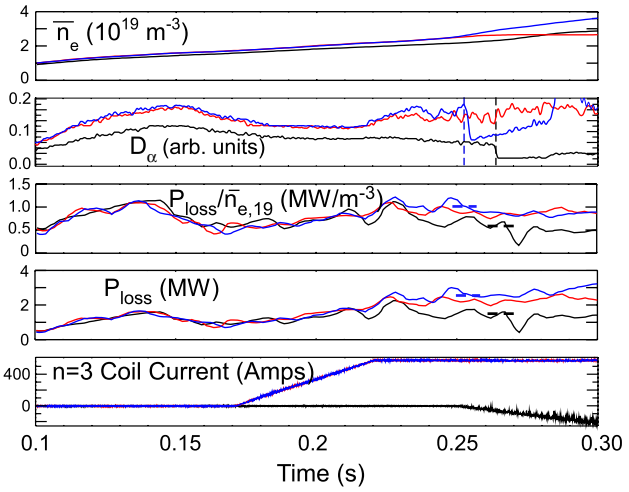

Figure 5. Waveforms for 0.9 MA, 0.44 T discharges with (blue, red) and without (black) $n = 3$ fields applied prior to the L–H transition. Shown from the top are line-averaged density, D_α emissivity, loss power normalized by line-averaged density, absolute loss power and $n = 3$ coil current.

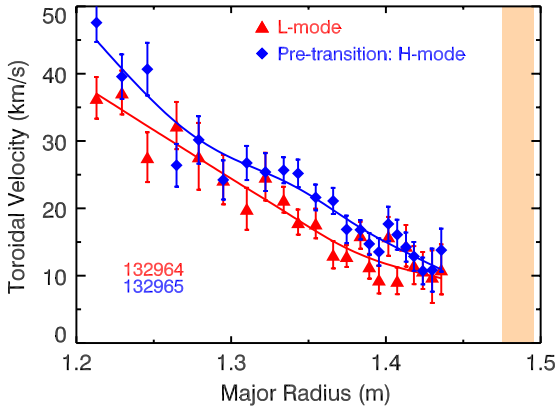

Figure 6. Toroidal carbon velocity for two discharges with applied $n = 3$ fields. The discharge denoted by the blue symbols transitioned into the H-mode, while that denoted by red symbols did not. The separatrix location, denoted by the shaded region, is given as a range due to uncertainties in this value as determined by equilibrium reconstructions.

(points) and the spline fits to the data (solid lines) for both the L-mode and pre-transition H-mode discharges at the same time in each discharge, which corresponds to 6 ms before the L–H transition in the pre-transition H-mode case. In the figure, the separatrix location is shown by the vertical shaded region, shown as a range to take into account uncertainties from the equilibrium reconstruction. Velocities only out to $R \simeq 1.44$ m can be measured due to the presence of C I emission outside this radius. As can be seen from the figure, the toroidal velocity for the discharge that remained in L-mode is lower than that for the pre-transition H-mode, although the values are comparable at 1.44 m. In addition, the toroidal velocity shear of the pre-transition H-mode discharge appears to be greater than that for the L-mode, as is seen in the spline fit. Poloidal velocities out to 1.44 m are significantly lower than the toroidal velocities, being $\leqslant 2$ km s^{-1} for both discharges. This difference is significant in determining the importance of each component in the radial electric field, E_r. In NSTX, the poloidal and toroidal magnetic fields (B_θ, B_ϕ) are comparable near the edge of the plasma. Through force balance, $E_r = f(v_\theta B_\phi, v_\phi B_\theta, \nabla p)$, which means that for small pressure gradient, which is the case for C VI in this region of the plasma, the E_r would be determined primarily by the toroidal velocity component in these NSTX plasmas. This result is consistent with results reported for high power H-mode discharges in NSTX [24]. At higher aspect ratio, the poloidal velocity and/or the pressure gradient can be important in determining E_r at the plasma edge [25–27]. For the discharges presented in this work, however, no conclusions can be drawn about the E_r or E_r shear beyond $R \simeq 1.44$ m, closer to the separatrix, due to the lack of data in that region. We do note that a single-point value of E_r can be inferred from toroidal and poloidal velocities of C III emission at $R \simeq 1.48$–1.49 m, and the E_r values for the two discharges at this location are comparable.

2.3. Effect of plasma current

A unique observation in NSTX is the dependence of power threshold on plasma current, a dependence that is not seen at higher aspect ratio. In neutral beam heated discharges at 0.7 MA, the L–H threshold power was determined to be $P_{loss} = 1.6$ MW, or 0.7 MW/10^{19} m^{-3} when normalized to line-averaged density. At 1.0 MA, the power threshold nearly doubled, increasing to 3.1 MW and 1.2 MW/10^{19} m^{-3} respectively, as is seen in figure 7. This scaling of P_{LH} with I_p is consistent with earlier observations in NSTX [28]. This result is also qualitatively consistent with the result that the power threshold at low aspect ratio depends on the total magnetic field at the edge [29]. According to the parameterization of the total field contained in that work, however, the difference in current should account for only a 30% increase in the threshold power reported here, while the observed increase is closer to a factor of two.

In an attempt to understand the source of this current dependence, XGC0 [20] calculations were performed. XGC0 determines the neoclassical radial electric field using input data that includes the toroidal rotation and it computes the particle losses self-consistently in the real magnetic geometry. The radial electric field for discharges that remain in the L-mode and that transition into the H-mode at the two current levels mentioned above are shown in figure 8. The L-modes are shown in the left panel, while the discharges that transition into the H-mode are shown in the right panel. For the discharges that do transition into H-modes, the times taken for the calculation are just prior to the L–H transition time. The same times were used for the discharges that remained in the L-mode (left panel). The error bars shown represent the range of uncertainty in the measured parameters important for determining the E_r. The lower current discharge clearly shows a deeper E_r well than that at the higher current for both the L-mode and pre-transition H-mode discharges. E_r wells for both the higher and lower current cases are shallower for discharges that remained in the L-mode. The E_r well difference is caused by the difference in thermal ion loss cone near the plasma edge for the two different currents. For the lower current, particles with energies up to 200 eV and with large $v_\parallel/v$ are preferentially lost relative to the higher current case, where the loss cone moves energies higher than the bulk of the ion population at that location.

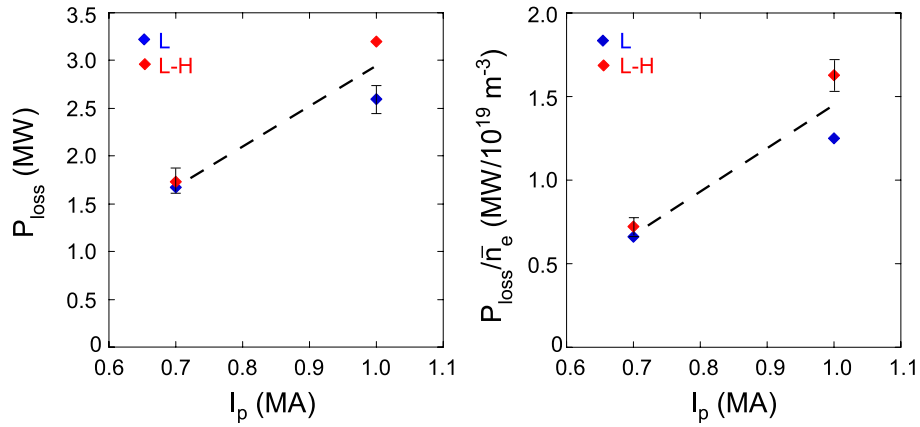

Figure 7. Loss power (left panel) and loss power normalized by line-averaged density (right panel) as a function of plasma current. Red symbols denote discharges that transition into the H-mode at that loss power, while blue symbols indicated discharges that remained in the L-mode for that loss power.

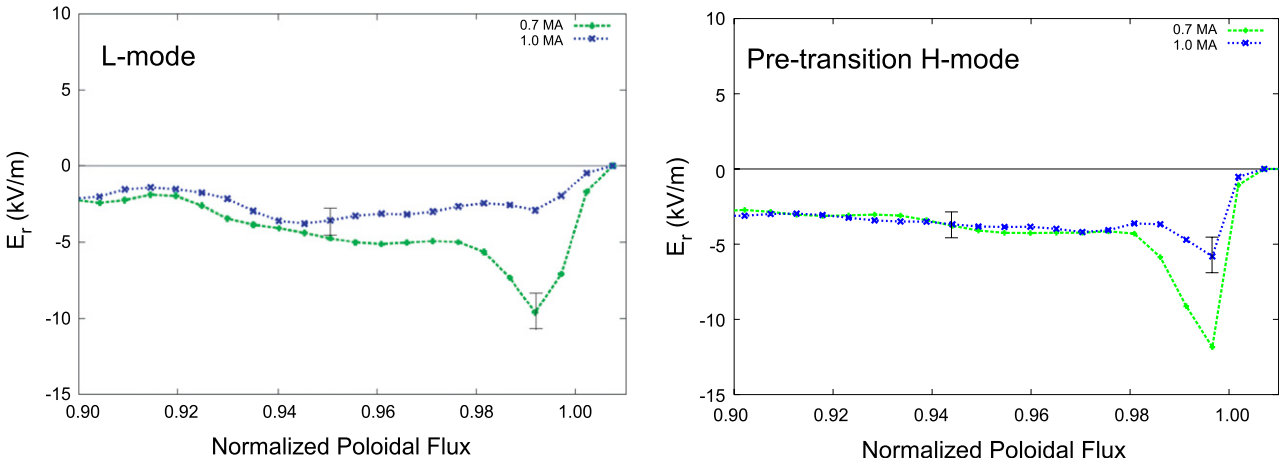

Figure 8. Neoclassical radial electric field as a function of normalized poloidal flux, as calculated in XGC0 for two discharges, at two different currents, that remained in the L-mode (left panel) and that transitioned into the H-mode (right panel).

It is not necessarily the difference in E_r well depth that makes the difference between whether or not a discharge transitions into the H-mode. The well depth of the low current discharge that did not transition (left panel) was computed to actually be deeper than that of the higher I_p discharge that did transition (right panel). Therefore, it might be something other than the difference in the E_r wells, such as a difference in the radial electric field shear, $\mathrm{d}E_r/\mathrm{d}r$, that may be most important. The E_r shear profiles for the set of discharges studied are shown in figure 9. As can be seen in the figure, the E_r shear for the lower current case is about a factor of two greater than that in the high current case for the discharges that transition into the H-mode ($\sim$8 versus $\sim$4 MV m^{-2}). On the other hand, the E_r shear values for those discharges that remained in the L-mode are both lower, although the lower current L-mode plasma still had an E_r shear value greater than that of the higher current L-mode ($\sim$4 versus $\sim$1 MV m^{-2}). Thus, it seems that for these discharges, $\sim$4 MV m^{-2} appears to be the E_r shear threshold necessary for achieving H-mode.

The dependence of P_{LH} on plasma current in NSTX but not at higher aspect ratio can be understood qualitatively by noting that the fraction of trapped particles increases with decreasing aspect ratio. Furthermore, the width of the banana orbit of

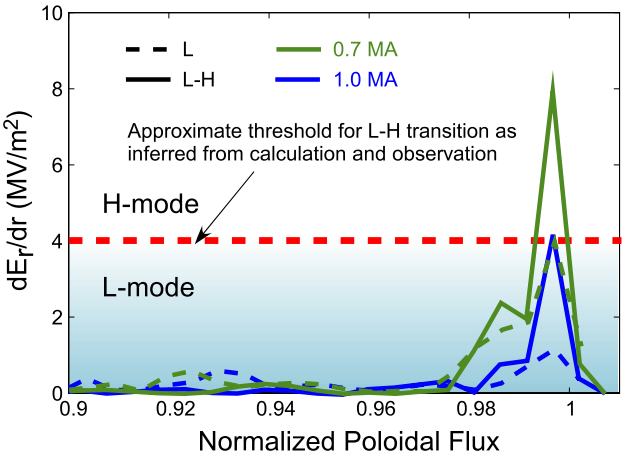

Figure 9. Neoclassical radial electric field shear as calculated by XGC0 for discharges in the current scan. The solid curves denote discharges that have transitioned into the H-mode at 0.7 MA (green) and 1.0 MA (blue), while the dashed lines denote discharges at those currents that remained in the L-mode. The approximate threshold in E_r shear is indicated by the red horizontal dashed line.

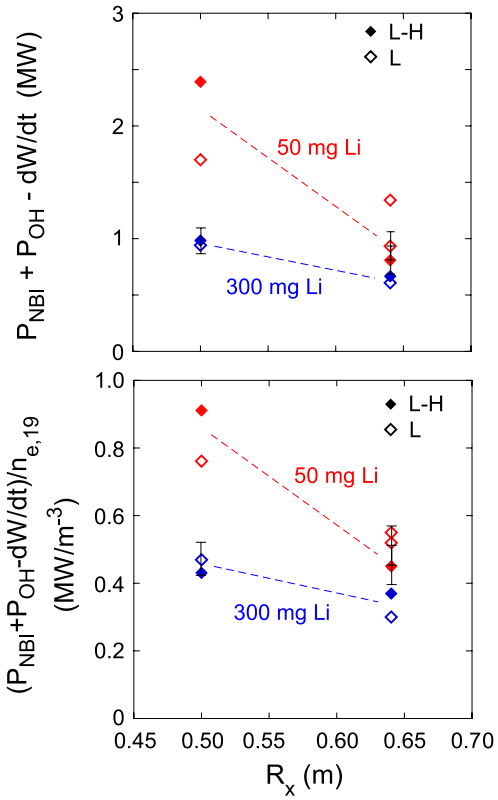

Figure 10. Loss power (top panel) and density-normalized loss power (bottom panel) as a function of X-point radius for two different lithium evaporation rates. The solid symbols denote discharges that have transitioned into the H-mode at that loss power, while the open symbols denote those that remain in the L-mode.

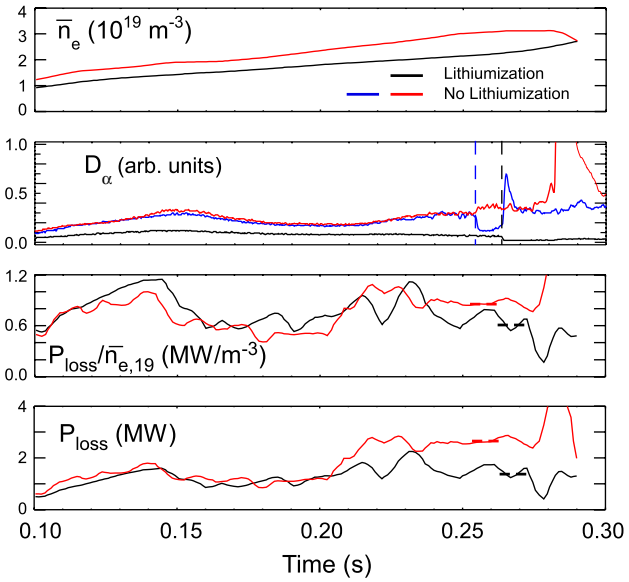

Figure 11. Comparison of discharges with lithium conditioning (red and blue) and without (black). Shown from the top are line-averaged density, D_α emissivity, density-normalized loss power and loss power. The discharge in blue, which transitioned into the H-mode was missing electron temperature and density profiles, but it was similar, as far as operational parameters, as the discharge in red which remained in the L-mode. The P_{LH} is therefore taken to be approximately the loss power of this discharge.

these particles is larger for particles with higher initial parallel velocity and for lower plasma current. In addition, the toroidal gyroradius of these trapped particles must also be taken into account, and NSTX operates at a toroidal magnetic field that is typically an order of magnitude less than that at higher aspect ratio. Given these features, the edge thermal ions in NSTX are more prone to loss than those at higher aspect ratio, and this may be why the sensitivity to plasma current is apparent at low aspect ratio.

2.4. *Effect of x-point location*

Motivated by XGC0 calculations which show strongest ion loss and largest edge E_r and E_r well or shear when the X-point is at large R, experiments assessing the L–H threshold power as a function of X-point radius, as reflected by differing triangularity were performed. Initial experiments exploring this dependence had mixed results due to secular variations in the magnitudes of P_{OH} and dW/dt as a function of triangularity [30]. A dedicated experiment was recently performed on NSTX to examine the triangularity (X-point radius) dependence of the L–H threshold controlling the above parameters as much as possible. Shown in the figure 10 are the results of the experiment done at two different lithium evaporation rates. Plotted are the loss powers (top panel) and density-normalized loss powers (bottom panel) as a function of X-point radius. The data clearly show a trend of lower threshold power at larger X-point radius (lower triangularity), consistent with the XGC0 results. While there was some shot-to-shot variability, the L–H threshold power was well determined in this experiment. Subsequent experiments showed that this dependence on X-point radius could be understood by the difference in the toroidal field at the two different X-locations (being higher for higher triangularity/lower R_x, thus leading to higher threshold power). In these experiments, the toroidal field was lowered in the high triangularity configuration to allow a comparison of P_{LH} at high and low triangularity at fixed B_{Tx} (B_T at the x-point location). For the same B_{Tx}, the power thresholds were comparable. Additional work to understand these results in the framework of thermal ion losses and neoclassical theory is underway [31].

2.5. *Effect of plasma conditioning*

The last global dependence to discuss is that on wall conditioning. NSTX has been utilizing between-shots lithium evaporation on the graphite plasma-facing components in an attempt to reduce recycling and control particle density. Typically, between 50 and 100 mg of lithium is deposited between plasma discharges, and this has resulted in increased electron and energy confinement and a suppression of ELMs in H-mode plasmas [19]. Use of lithium has led to a significant reduction in the L–H power threshold as well. A comparison of two similar discharges, but one with lithium conditioning and one without and after the lithium conditioning effects wore off, showed that without lithium, $P_{LH} \sim 2.7$ MW, but with lithium, $P_{LH} \sim 1.4$ MW (figure 11). It should be noted that the discharge with lithium had significantly lower density, so a better comparison is with $P_{LH}/\bar{n}_e$, and here the discharge without lithium had a threshold of 0.9 MW/10^{19} m^{-3}, while the one with lithium conditioning

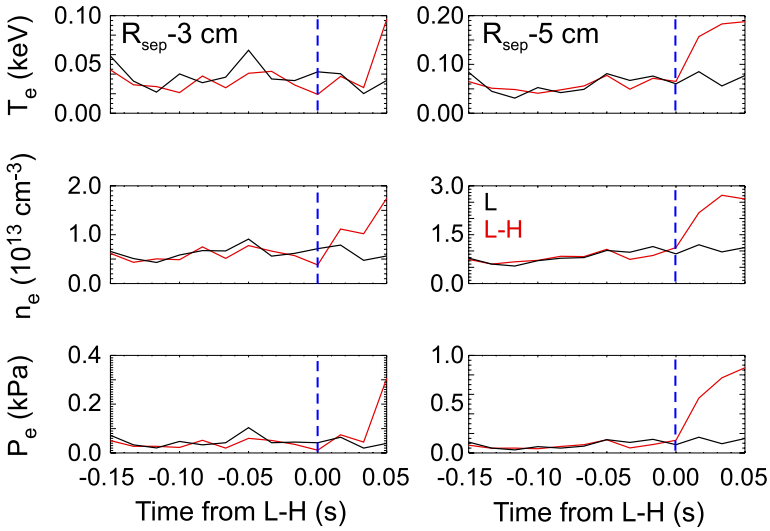

Figure 12. Evolution of the electron temperature, density and pressure at two radial positions, 3 and 5 cm inside the separatrix, for a discharge that transitions into the H-mode (red) and one that does not (black).

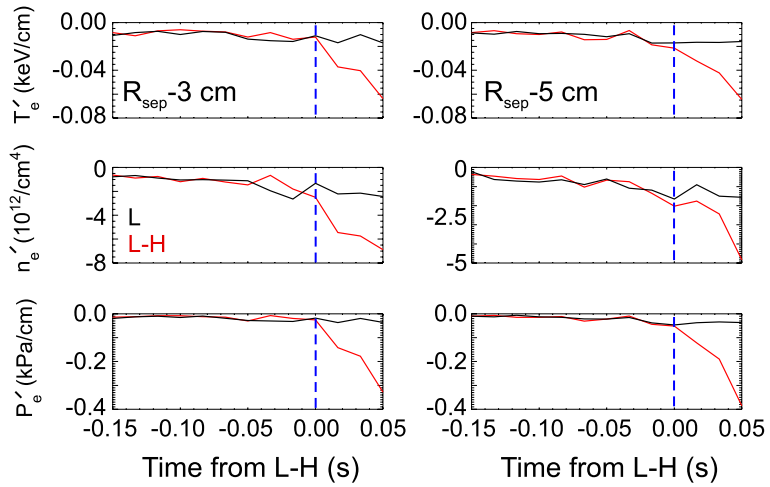

Figure 13. Evolution of the gradients in the electron temperature, density and pressure at two radial positions, 3 and 5 cm inside the separatrix, for a discharge that transitions into the H-mode (red) and one that does not (black).

had a threshold of 0.55 MW/10^{19} m^{-3}. This trend is supported by the difference in P_{LH} between discharges with high and low lithium evaporation rates shown in figure 10. Further analysis is underway to attempt to understand the cause of this difference, including the effect of differing neutral density on the threshold power [32].

3. Effect of local parameters on the L–H transition

It is widely believed that the physics behind the L–H transition is tied more to local than to global processes. While the global heating power parameter may be a reasonable characterization for knowing approximately what is needed for H-mode access, there are effects that are not reflected and difficult to quantify using this global approach. Therefore, it has become more apparent that the study of how local edge parameters and their gradients change leading up to the L–H transition may yield insight into the underlying physics [7–11]. This was seen in the earlier discussion of E_r shear, for instance [13, 12, and references therein]. The measurement of the local edge parameters in NSTX is, at this time, limited in terms of temporal and to some extent spatial resolution. The Thomson scattering diagnostic (T_e, n_e) has temporal and spatial resolution of 16 ms and 1.5 cm respectively, while the CHERS (T_i, v , n_{carbon}) has 10 ms, 1 cm resolution. Because of this, only the longer-time scale changes can currently be studied on NSTX; diagnosing changes on or below the time scale of ms is not possible.

A statistical study, using approximately 20 discharges, was performed. In particular, the evolution of discharges with similar operational parameters, but in which one transitioned into the H-mode while the other did not, was compared in detail. Examples of this comparison are shown in figures 12 and 13, and the conclusions are representative of all comparisons made. Plotted in figure 12 are the time traces of the electron temperature, density and pressure plotted as a function from time of transition for a discharge that transitioned into the H-mode at $t = 0.0$ s (red) and one that did not (black). Here, the time base for the L-mode discharge was the same as for the one that transitioned into the H-mode. Traces are

plotted at radial positions 3 and 5 cm inside the separatrix. As can be seen, no difference in these local quantities, to within the spatial and temporal resolution of the data, is seen for either radial position. Once in the H-mode, the discharge shown in red clearly shows an increase in these quantities, reflecting the buildup of the edge gradients, but this occurs after the transition [33].

The gradients of these quantities at these two radial positions are shown in figure 13, and again, to within the data resolution, no difference can be seen between the L and the L–H discharge prior to the transition. These results, in addition to those discussed in the previous section, do not support there being a profile-change precursor to the L–H transition to the time resolution available in this data set.

4. Confinement quality following the L–H transition

The initial ITER heating capabilities are expected to provide enough power for transition into the H-mode, although given the uncertainties in the power threshold, the power level may not exceed $P_{\rm LH}$ by very much. This raises two important issues. The first is whether, once the discharge transitions into the H-mode and density begins to rise, can the discharge remain in H-mode? The NSTX results reported in the previous sections indicate that, using the strict definition of $P_{\rm loss}$ (i.e. with the $\mathrm{d}W/\mathrm{d}t$ term included), the H–L transition occurs at the same normalized power as the L–H transition, indicating potential difficulty in remaining in the H-mode at constant power but increased density. Without the inclusion of the $\mathrm{d}W/\mathrm{d}t$ term in this definition, hysteresis exists, and the discharge is able to remain in the H-mode even below the nominal L–H threshold power. It is important to minimize the variation of $\mathrm{d}W/\mathrm{d}t$, and additional experiments will be carried out to address this.

The other issue has to do with the confinement quality at powers just above the L–H threshold. The confinement quality is typically $H_{98y,2} \sim 0.8$ in discharges that exhibit type III ELMs just above the power threshold [23, 34, 35]. The HHFW and NBI-heated discharges presented in this work were used to assess the confinement quality for $P_{\rm loss} \simeq P_{\rm LH}$, and to attempt to understand the conditions under which the confinement quality is optimized. As was seen in figure 1, the HHFW discharges tended to last for only a few hundred msec, and the power was decreased shortly after the discharge transitioned to the H-mode. Consequently, for these discharges, the confinement quality at $P \simeq P_{\rm LH}$ could be assessed at a time only tens of msec after the transition. Neutral beam heated discharges lasted longer, and thus the confinement quality could be assessed over a duration lasting up to hundred of msec after the transition, depending on the total duration of the discharge.

The confinement quality, in terms of $H_{98y,2}$, as a function of time after the L–H transition are shown in figure 14. In all of these discharges, ELMs were suppressed from the between-shot lithium conditioning. The net heating powers in these discharges were mostly within 5% to 10% of the threshold power. $P_{\rm loss}$, as defined earlier in the paper, were used to calculate both τ_E and $\tau_{98y,2}$ for the determination of $H_{98y,2}$. The uncertainties in the confinement enhancement factor due to uncertainties in the heating powers and the stored energy are shown in the plot. Even within these relatively large

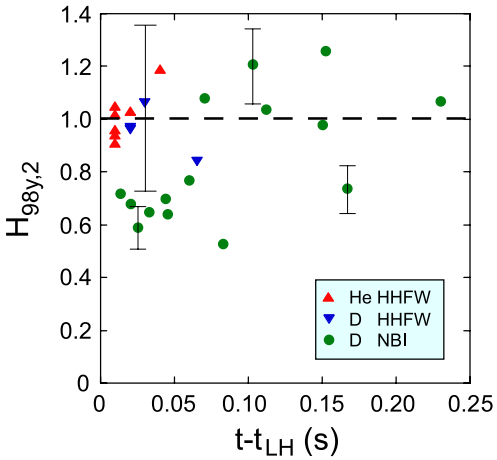

Figure 14. Confinement quality as a function of time from transition for HHFW and NBI-heated discharges.

uncertainties, it is seen that $H_{98y,2} \sim 1$ confinement can be obtained just after the L–H transition. This is most clearly seen in the HHFW heated discharges, where $H_{98y,2} \sim 1$ is seen within 10 ms of the transition. For the neutral beam heated discharges, the H-factors are lower at this time, but they increase to $H_{98y,2} \sim 1.0$ and above within approximately 50 ms of the transition, as the density increases. The 50 ms represents approximately two fast ion slowing down times.

There is some variation seen in the confinement time enhancement factors even once the discharges have achieved a 'steady-state' in this parameter. The precise recipe for obtaining the highest H-factors is not fully understood, although the NSTX data do indicate that plasma shaping is extremely important. The H-factors are found to be higher with higher elongation or triangularity (the two are inseparable in these NSTX experiments). Additional experiments are planned to identify the controlling factors.

5. Summary and conclusions

Dedicated NSTX experiments on the L–H power threshold have contributed to the ITER and ITPA high priority physics requests on this topic. It was found that the L–H threshold power for helium was 20 to 40% greater than that for deuterium at a line-averaged density of $\sim 2.2 \times 10^{19}$ m^{-3}, and that is within the range of acceptability for ITER operation. It was also shown that wall conditioning using lithium can ease access to the H-mode significantly. On the other hand, there is a potential complication with utilizing an ELM suppression system which applies low-n magnetic perturbations to the plasma edge in a preventative mode prior to the transition, as this can result in at least a 50% increase in power threshold. Further, it appears that low triangularity plasmas are required for minimizing the power threshold. Unique to NSTX is the current dependence of the L–H threshold power; the sensitivity to this parameter in NSTX, and not at higher aspect ratio, is consistent with the higher trapping fraction and larger toroidal gyroradius at low aspect ratio. Theoretical calculations based on neoclassical theory indicate that for these plasmas there appears to be an E_r shear threshold of approximately 4 MV m^{-2} for effecting a transition into the H-mode for the discharges studied. To

within the spatial and temporal resolution of the relevant diagnostic systems on NSTX, no difference in edge density or temperature, or their gradients, was observed when comparing discharge periods leading up to the L–H transition, with those that remained in L-mode. There is some indication that the rotational shear in the outer portion of the plasma is greater in discharges that transition into the H-mode (just before the transition) than in those that remain in the L-mode. Finally, $H_{98y,2} \sim 1$ confinement quality could be obtained just after the L–H transition for HHFW heated discharges and within one to two slowing down times for neutral beam heated discharges in ELM-free conditions. The precise recipe for obtaining this good confinement, which depends on plasma shaping and discharge evolution, is still under study.

Acknowledgments

This work has been supported by US Department of Energy Contract Numbers DE-AC02-09CH11466 and DE-AC05-00OR22725.

References

[1] Wagner F.G. *et al* 1982 *Phys. Rev. Lett.* **49** 1408
[2] Kaye S.M. *et al* 1984 *J. Nucl. Mater.* **121** 115
[3] ITER Confinement Database and Modeling Group 1997 *Proc. 16th Int. Conf. on Fusion Energy 1996 (Montreal, Canada, 1996)* (Vienna: IAEA) vol 2, p 795
[4] Martin Y.R., Takizuka T. and the ITPA CDBM H-Mode Threshold Working Group 2008 *J. Phys.: Conf. Ser.* **123** 012033
[5] The ASDEX Team 1989 *Nucl. Fusion* **29** 1959
[6] Kaye S.M. *et al* 2006 *Nucl. Fusion* **46** 848
[7] Hubbard A. *et al* 1998 *Plasma Phys. Control. Fusion* **40** 689
[8] Hubbard A. *et al* 2007 *Phys. Plasmas* **14** 056109
[9] Suttrop W. *et al* 1999 *Plasma Phys. Control. Fusion* **41** A569
[10] Andrew Y. *et al* 2006 *Plasma Phys. Control. Fusion* **48** 479
[11] Groebner R.J., Thomas D.M. and Deranian D. 2001 *Phys. Plasmas* **8** 2722
[12] Connor J. and Wilson H.R. 2000 *Plasma Phys. Control. Fusion* **42** R1
[13] Diamond P.H. *et al* 1994 *Phys. Rev. Lett.* **72** 2565
[14] Diamond P.H. *et al* 2005 *Plasma Phys. Control. Fusion* **47** R35
[15] Moyer R.A. *et al* 2001 *Phys. Rev. Lett.* **87** 135001
[16] Estrada T. *et al* 2009 *Plasma Phys. Control. Fusion* **51** 124015
[17] Conway G.D. *et al* 2011 *Phys. Rev. Lett.* **106** 065001
[18] Sontag A.C. *et al* 2007 *Nucl. Fusion* **47** 1005
[19] Kugel H.W. *et al* 2008 *Phys. Plasmas* **15** 056118
[20] Chang C.S., Ku S. and Weitzner H. 2004 *Phys. Plasmas* **11** 2649
[21] Ryter F. *et al* 2009 *Nucl. Fusion* **49** 062003
[22] Gohil P. *et al* 2010 L–H transition studies in DIII-D to determine H-mode access for non-nuclear operational scenarios in ITER *Proc. 23rd Fusion Energy Conf. (Daejeon, South Korea, 2010)* Paper EXC/2-4Ra http://www-pub.iaea.org/MTCD/Meetings/PDFplus/2010/cn180_papers/exc_2-4ra.pdf
[23] McDonald D.C. *et al* 2010 JET Helium-4 ELMy H-mode studies *Proc. 23rd Fusion Energy Conf. (Daejeon, South Korea, 2010)* Paper EXC/2-4b http://www-pub.iaea.org/MTCD/Meetings/PDFplus/2010/cn180_papers/exc_2-4rb.pdf
[24] Bell R.E. *et al* 2010 *Phys. Plasmas* **17** 082507
[25] Bell R.E. *et al* 1998 *Phys. Rev. Lett.* **81** 1429
[26] Gohil P. *et al* 1998 *Nucl. Fusion* **38** 93
[27] Kamiya K. *et al* 2010 *Phys. Rev. Lett.* **105** 045004
[28] Bush C.E. *et al* 2003 *Phys. Plasmas* **10** 1755
[29] Takizuka T. and the ITPA H-mode Power Threshold Database Working Group 2004 *Plasma Phys. Control. Fusion* **46** A227
[30] Maingi R. *et al* 2010 *Nucl. Fusion* **50** 064010
[31] Battaglia D. 2011 *Nucl. Fusion* to be submitted
[32] Lee K.C. 2006 *Phys. Plasmas* **13** 062505
[33] Kaye S.M. *et al* 2003 *Phys. Plasmas* **10** 3953
[34] Saibene G. *et al* 2002 *Plasma Phys. Control. Fusion* **44** 1769
[35] Ryter F. *et al* 2008 *J. Phys.: Conf. Ser.* **123** 012035